IIETA International Information and Engineering Technology Association
Advancing the World of Information and Engineering

Annales de Chimie - Science des Matériaux
Vol. 47, No. 6, December, 2023, pp. 363-369
Journal homepage: http://iieta.org/journals/acsm

Analyzing Self-Compacted Mortar Improved by Carbon Fiber Using Artificial Neural Networks

Ahmed Mohamad Ahmed[1], Safaa Ibrahim Ali[1], Muataz Ibrahim Ali[1*], Asmaa Abdul Jabbar Jamel[2]

[1] Department of Civil Engineering, College of Engineering, University of Samarra, Samarra 34010, Iraq
[2] Department of Civil Engineering, College of Engineering, University of Tikrit, Tikrit 34001, Iraq

Corresponding Author Email: mutaz.ibrahim@uosamarra.edu.iq

https://doi.org/10.18280/acsm.470602

Received: 26 August 2023
Revised: 13 October 2023
Accepted: 23 October 2023
Available online: 22 December 2023

Keywords:
artificial neural networks, self-compact mortar, ANN, carbon fiber, fresh properties, SCM, mini funnel, diameter of flow

ABSTRACT

This study presents an analytical framework, employing artificial neural networks (ANNs), to characterize the fresh properties of self-compacting mortar (SCM) reinforced with 6mm long carbon fibers at varying content ratios (0.05, 0.1, 0.2, and 0.4% by weight). Utilizing a multi-layered network approach with reactive error variance, the analysis delivers a nuanced understanding of the influence carbon fibers exert on SCM's fresh characteristics. It was observed that the inclusion of carbon fibers extended the passage time through a mini funnel and contracted the flow diameter, indicating alterations in workability. The ANN model demonstrated a high degree of predictive accuracy for fresh SCM properties, achieving a validity of 97.5% and a coefficient of determination (R^2) of 89.4%.

1. INTRODUCTION

Cement-based fillers are recognized for their ability to self-compact, rapidly achieving in situ flow without segregation, and demonstrating substantial filling capacity. The mobility of cement grout is crucial for ensuring cohesion and preventing segregation during flow, thereby producing homogenous grout [1]. The vibrational compaction of liquid cement grout is not required, which can lead to reductions in labor and equipment use, enhancing compaction efficiency and increasing the durability of structural elements' cover regions [2]. A fundamental aspect of grouting techniques is the injection and subsequent solidification of adequate fluid into the voids that require grouting, which is particularly advantageous for concrete filling in complex mold geometries.

Despite these benefits, self-compacting mortar (SCM) incurs higher primary material costs compared to conventional concrete. The challenge lies in the need for chemical admixtures and high cement volumes to achieve mixtures with adequate mobility and durability [3]. SCM formulations require large powder ratios with lower water-to-binder ratios and extensive use of superplasticizers [4]. Although increased paste content can enhance workability, it may negatively impact mechanical properties and contribute to time-dependent deformations. Notably, both drying shrinkage and autogenous shrinkage escalate with the increase in paste volume [5, 6], making the shrinkage of cement-based mixtures dependent on the cement content.

Fibers, such as carbon fibers, have been incorporated into cement to improve the tensile strength and durability of concrete. These fibers serve to bridge cracks and inhibit their propagation. The efficacy of fibers is contingent upon their aspect ratio and volume fraction [7]. Carbon fibers, possessing chemical stability, high specific strength, and elastic modulus, are deemed suitable for concrete applications [5]. Incorporation of carbon fibers into cement mixtures has been documented to elevate tensile and flexural strength, diminish dry shrinkage, and bolster the bond strength of the concrete mixture [8, 9]. The enhancement of mixture properties with the addition of carbon fibers is contingent on the fiber content, provided that no excess air voids are introduced, which could detrimentally affect compressive strength. Conversely, the inclusion of fibers can detract from the workability of the mixture. Thus, the effective utilization of carbon fibers in mortar necessitates their homogeneous distribution within the matrix [9-11].

Artificial neural networks (ANNs), mirroring biological neuronal networks, enable the simplification of complex, nonlinear phenomena [12]. Neural networks are considered efficacious for a multitude of applications, particularly in addressing intricate issues within civil and structural engineering that involve numerous inputs [13, 14].

The architecture of artificial neural networks (ANNs) typically adheres to a uniform framework. A quintessential configuration of neurons within a layered assembly is depicted in Figure 1, where the initial layer—the input layer—captures the essential parameters or input variables. These inputs may be gleaned directly from electronic sensors or derived from input files. The output layer, dictated by the quantity of predictive elements or categories, transmits information to external interfaces or systems, such as a mechanical control apparatus or a parallel computational device. The intermediary layers, known as hidden layers, comprise numerous units arrayed in varied configurations of interconnectivity. The

model presented in Figure 1 delineates N inputs leading to a singular output, with the summation junction (∑) and the transfer functions *f* located within the core of each neuron. The artificial neurons utilize predefined settings and variables [15].

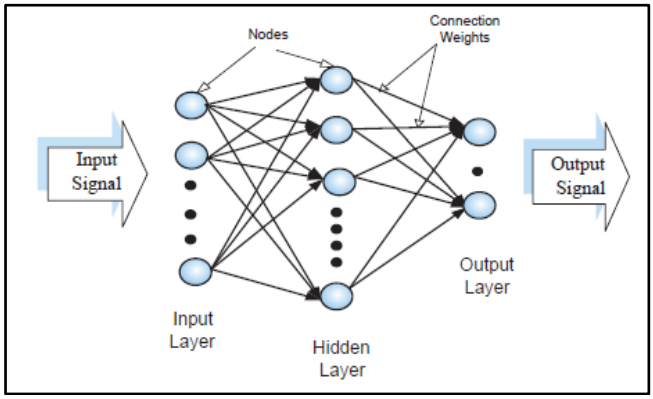

Figure 1. Architecture of the neural network

Each input is assigned a specific weight, which exerts the requisite influence for the summative analysis of the inputs. The internal bias (b) of the network, a fixed element, signifies the degree of shift influencing the activation threshold of the neuron's output. The input vectors and the corresponding weight vectors are represented as ($x_1, x_2, ..., x_N$) and ($w_1, w_2, ..., w_N$), respectively. The summation function is computed by the dot product of vectors x and w, followed by the addition of the bias, as expressed in Eq. (1).

$$a = \sum_{i=1}^{N}(w_i\, x_i) + b \qquad (1)$$

The output will be a single value. This normalized result from the summing function can be converted to the functional output using a transfer function. Once neurons are adequately active, their output equals 1, but if not activated enough, their output equals zero. In neural networks, numerous activation functions are employed to determine the neuron output to a specific input [15, 16].

This research aims to develop self-compacting mortar (SCM) by employing carbon fibers (CF) to optimize the characteristics of fresh concrete mortar and statistically analyze results using artificial neural networks (ANN), then determine an algebraic model that investigators may utilize.

2. EXPERIMENTAL PROGRAM

The self-compacted mortar was designed using the European Code (EFNARC) [17]. Twenty-five mixtures were prepared with five different water-to-cement ratios, and every water-to-cement ratio has five different fibers-to-cement ratios; the first mixtures contained no carbon fibers (reference mix), and the remaining four ratios of fiber to cement by weight were (0.05%, 0.1%, 0.2% and 0.4%), as shown in Table 1. The SP content was 1% of cement mass, and the mortar was mixed using the (Walraven & Grunewald) method [18]. The cement and sand were mixed for 10 seconds at first, then the water and superplasticizer were added, and the mixing continued for 110 seconds; after that, the carbon fiber was added, and mixing continued for an additional 90 seconds.

Table 1. The specifics of the self-compacting mortar mixes

Mix. Name	w/c*	f/c**	s/c***	sp/c****
M.1	0.55	0	1.700	1
M.2	0.55	0.05	1.699	1
M.3	0.55	0.1	1.698	1
M.4	0.55	0.2	1.697	1
M.5	0.55	0.4	1.694	1
M.6	0.57	0	1.700	1
M.7	0.57	0.05	1.699	1
M.8	0.57	0.1	1.698	1
M.9	0.57	0.2	1.697	1
M.10	0.57	0.4	1.694	1
M.11	0.6	0	1.700	1
M.12	0.6	0.05	1.699	1
M.13	0.6	0.1	1.698	1
M.14	0.6	0.2	1.697	1
M.15	0.6	0.4	1.694	1
M.16	0.62	0	1.700	1
M.17	0.62	0.05	1.699	1
M.18	0.62	0.1	1.698	1
M.19	0.62	0.2	1.697	1
M.20	0.62	0.4	1.694	1
M.21	0.65	0	1.700	1
M.22	0.65	0.05	1.699	1
M.23	0.65	0.1	1.698	1
M.24	0.65	0.2	1.697	1
M.25	0.65	0.4	1.694	1

w/c* water to cement ratios
f/c** fiber to cement ratios
s/c*** sand to cement ratios
sp/c**** Super plasticizer to cement ratios

3. COMPONENT CHARACTERISTICS

3.1 Cement

Ordinary Portland Cement (OPC) was used in all the mixtures of this research. The physical properties and chemical composition of cement correspond to Iraqi specification No. 5/1984.

3.2 Fine aggregate

The sand utilized in this research paper achieved the Iraqi Standard No. (45) – 1984 [19] grading requirements lie within the third area.

3.3 Superplasticizer

In this research paper, the superplasticizer was a high-quality chloride-free with technical characteristics that conform to ASTM C494 [20].

3.4 Carbon fiber

Table 2. Carbon fibers' physical characteristics

Description	Details
Length (mm)	6
Geometry	Fibrillated
Density (Kg/m^3)	910
Diameter (mm)	0.02
Tensile Strength (MPa)	400
Modulus of Elasticity (MPa)	3450

The carbon fibers employed in the study are extremely efficient fibers characterized by high tensile strength and high elasticity, which were brought as mats and cut into 6 mm in length and were used as single strips. The characteristics of these fibers are shown in Table 2.

4. FRESH SELF-COMPACT MORTAR TESTS

4.1 Mini flow test

This test is conducted to evaluate the horizontal flow of the self-compacting mortar and is used. The test is to cast the self-compacted mortar in a broken cone with (100*70*60) mm (bottom*top*height), respectively. The cone should be constructed of a smooth surface texture and placed on a solid structure of the same cone material. After mortar casting is finished, the cone is lifted vertically, and the diffusion diameter is measured; the average of two orthogonal readings is considered. This test does not measure the ability of the mortar to pass between obstacles without clogging. It gives a trend of segregated resistance of the mortar. Mini flow check test details are shown in Figure 2.

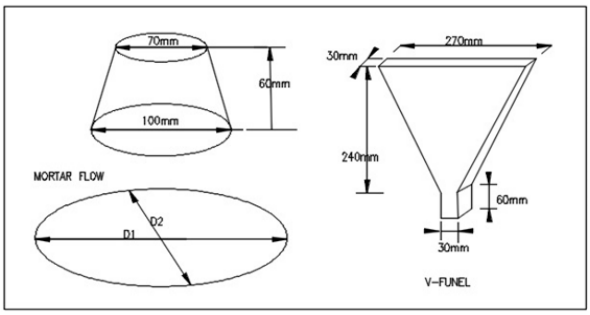

Figure 2. Dimensions of mini-slump and mini V-funnel

4.2 Mini V-funnel test

This test is conducted to measure the fallibility of the self-compact mortar, mortar viscosity, and flow ability of the mortar. The test includes casting one litter of the self-compacting mortar through a V-shaped funnel and measuring the time the mortar passes through the funnel. The details of the mini V-funnel are shown in Figure 2.

5. MODEL DEVELOPMENT BY ANNS

The ANN was used to analyze and estimate the effect of the variables on the results of the fresh self-compact mortar by determining the variables entered in the ANN, so simulations using a computer model to predict the fresh properties for SCM.

Neural networks have several types of self-regulated Pyreptron, Cohon networks, and feed-forward neural networks [21, 22]. This research used back-propagation feed-forward, which contains a group of neurons arranged in layers. These neurons are usually connected; every neuron in one layer is linked to every neuron in the next layer (the neurons of the same layer are not connected). The typical form of these networks is at least three neural layers (input layer, hidden layer, and output layer); the input layer is unprocessed. It is simply the place where the network feeds the data radiation. Then, the input layer feeds (information transfer) the hidden layer. After that, the hidden layer feeds the output layer.

The ANN used in this research consists of sub-models such as the input model, output model, data division model, model selection of neural network architecture, model weight, and validation model. The SPSS program was used, which was one of the applications used for artificial intelligence techniques and the construction of various artificial neural networks. This program illustrated the sub-models from the input to the output model.

6. RESULTS AND DISCUSSION

6.1 Experimental study

6.1.1 Flow ability

Figure 3 has shown for the same water/cement ratio (w/c), a flow is decreased by an increasing fiber/cement ratio (f/c) and reducing the aggregate/cement ratio (s/c), where size of a flow is 247 mm since there is no fiber and (228, 225, 220, and 205 mm) when fibers ratio is more excellent respectively by 0.05, 0.1, 0.2, and 0.4%, Once the water/cement ratio exceeds 0.55, it exceeds the limitations of the European code (EFNARC).

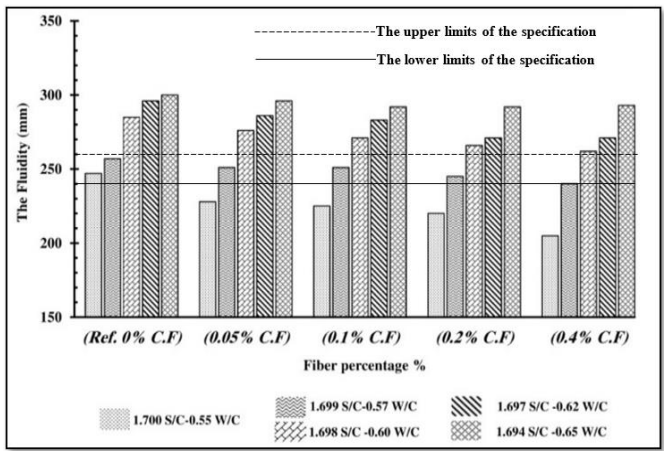

Figure 3. The relationship involving workability and fiber proportion

When w/c is 0.57, the flow diameter is 257 mm when there is no fiber. This quantity begins to decrease by gradually increasing the fiber ratio by (0.05, 0.1, 0.2, and 0.4%) of the weight of the cement to give a flow of 251,251, 245, and 240 mm, respectively, within standard boundaries of (240 to 260) mm.

The flow ratio is higher than the upper limit of 260 mm since the flow's diameter is between 262 mm and 300 mm. The reason for the decrease in flow, once the fiber ratio increased, is to increase the proportion of the surface area of fiber with increasing quantity in the mixture as well as to increase the possibility of intertwining the fibers between each other as well as between them and aggregates increase the internal resistance to the flow of fresh mortar. The variable (sp/c) is not used because it is constant in all mixes.

6.1.2 Flow time

Figure 4 shows the flow time at the same water-to-cement ratio (w/c) since it is clear from the Figure that adding fiber increased V-funnel compared to non-fiber mixtures. This

change is related to increasing fiber surface area and hence the flow ability of these mixes, and also high carbon fiber's tendency to restrict the flow between aggregates and fiber, increasing friction between them.

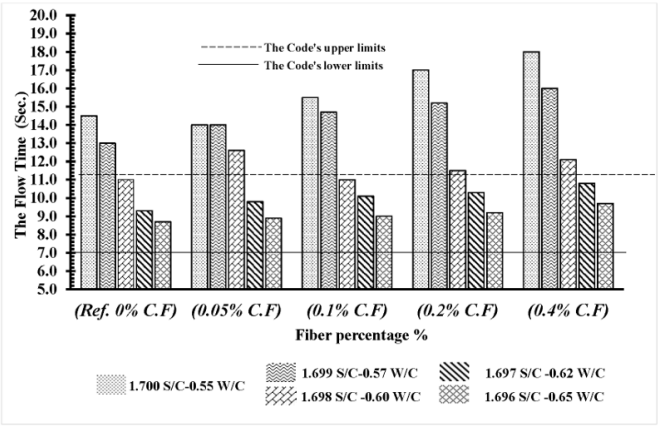

Figure 4. The connection involving flow time and fiber ratio

It is noted that increasing the fiber content for cement (f/c) from 0.05% to 0.4% leads to a significant increase in the fiber content of the mixture. In the viscosity of the self-adhesive mortar. This viscosity is also associated with the time of the suppression test, increasing the time required to pass from the funnel. When the (w/c) ratio of 0.55 is observed, the passage time of the suppression increases by increasing (f/c) and decreasing the proportion of (s/c) where the test time is 14.5 seconds when the mixture does not contain fiber, 14, 15.5, 17 and 18 seconds when the fiber ratio increased by 0.05, 0.1, 0.2 and 0.4% of cement weight, respectively.

When (w/c) is 0.57, the suppression time is 13 seconds when the mixture does not contain fibers. The time is 14, 14.7, 15.2, and 16 when the percent of (f/c) is increased by 0.05, 0.1, 0.2, and 0.4%, where the increased value exceeds the code (EFNARC) maximum limit of 11 seconds. These values continue to decrease with the increase of (w/c), where the value of the decrease exceeds the code (EFNARC) maximum limit of 11 seconds when (w/c) is 0.60 and remains within the limits of the specification in the percent of water /cement 0.62 and 0.65. So, the variable (sp/c) is not used because it is constant in all mixes.

6.2 Statistical study using ANNs

6.2.1 Flow ability

The input data in the input model includes independent variables (w/c), (f/c), and the ratio of sand to cement (s/c). In contrast, the output data was the diameter of fluidity (flow) of the self-compact mortar (SCM). Divided data into three groups: the training group to adjust the weights that contact with ANNs, the testing group to ensure the network's performance, so the training is stopped when the error increases at the testing group, and the validation group is used to evaluate the model's performance.

Table 3 shows the ratio of the data distribution for the three groups using the trial and error method to get the best performance of the ANNs by reaching the maximum correlation coefficient (r) to show the accuracy of the relationship between the output of the network (the predicted diameter of flow), with actual flow diameter. From Table 3 we note that the best classification of data is (88%) for the training group, (8%) for the testing group, and (4%) for the validation group based on the lowest ratio for testing error (2%) and the most significant correlation coefficient (96.6%).

Table 3. The effect of data division on the performance of the ANNs

Data Division			Training Error%	Testing Error%	Coefficient Correlation (r)%
Training%	Testing%	Validation%			
76	21	1	7.6	11.8	96.7
60	20	20	9.5	21.1	94.4
76	12	12	6.1	8.5	96.8
80	12	8	6.3	10.1	96.6
88	8	4	7.9	2	96.6
80	16	4	7	6.7	96.1
84	12	4	13.5	2.8	93.9
68	20	12	8.5	4.7	95.6
72	16	12	7.8	33.1	94.9
68	16	16	8	9.7	95.2

To distribute the 25 samples into the three groups, the program offers efficient methods for distributing the data in many ways (random, striped, and integrated package (blocked)). The striped method was selected because it gives the highest coefficient of correlation and the lowest error ratio.

The number of neural nodes in the input layer is three nodes; the output layer consists of a single neural node, which is the diameter of the flow. So, many methods are used to find the optimal number of nodes in the ANNs. The best way to find it is to use Eq. (1), which includes selecting one node in the hidden layer and gradually increasing the neural nodes until the network's best performance is reached. So, the maximum number of the neural nodes equals 7 according to Eq. (2).

$$Max.No.of\ Node = 1 + 2 \times I \quad (2)$$

where, I is the count of parameters on the input layer.

Table 4. The impact of the number of neurons in the hidden layer on ANN efficiency

No. of Nodes	%Training Error	%Testing Error	Coefficient Correlation (r)%
1	7.9	2	96.6
2	5	12.8	97
3	5.9	12.1	96.6
4	9.4	4.1	96.1
5	7.2	20.9	96.3
6	6.2	3.3	96.8
7	6.5	3.4	97.2

Table 4 shows the ratios of the correlation coefficient and

testing error for the middle layer (hidden layer), which was based on the learning rate of 0.4 and the momentum term equal to 0.9, so the transfer function for the middle layer was sigmoid. Table 4 notes that the best performance of the ANNs is when the number of neural nodes in the hidden layer is equal to one neural node because it has the maximum coefficient of correlation (96.6%) and the lowest error ratio (2%). Consequently, there were three neural units in the input layer, one in the hidden layer, and one in the output layer, which is the expected diameter of the flow.

When noting the weights of contact (every connection between a neuron and another with a value is called weight), this value shows the importance of the correlation between these two elements; the neuron multiples each input value from neurons of the previous layer by the weights of the connection with these neurons, after that the neuron collects all the multiplication.

After training the ANNs, the weights of neural nodes were obtained; it was interactions between both the input and hidden layers, in addition to neural node weights connecting the hidden layer and output layer., as shown in Figure 5, which shows the weights of the bond between the layers and the thresholds limit of the hidden layer and the output layer.

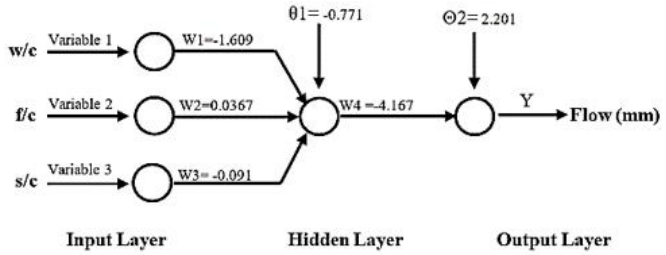

Figure 5. The neural network architecture model

The predicted value of the diameter of the flow for the SCM containing the carbon fiber by using Eq. (3):

$$y = \frac{1}{1 + e^{-(\theta 2 - w4 * \tanh(X))}} \tag{3}$$

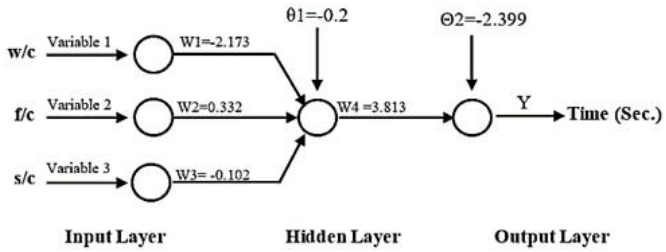

Figure 6. The neural network architecture model for flow time

So, by using the weights (Wi) and the thresholds limit (θ1) and (θ2) shown in Figure 6, we get the Eq. (4):

$$y = \frac{1}{1 + e^{-(2.201 + 4.167 * \tanh(X))}} \tag{4}$$

where, Y is diameter of flow (fluidity).

The variable (X) can be found in the Eq. (5):

$$X = \theta 1 + (W1 * V1) + (W1 * V2) + (W1 * V3) \tag{5}$$

where,

V1: Water-to-cement ratio (w/c).

V2: Fiber contains to cement (f/c)

V3: Ratio of sand to cement (s/c)

The variable (sp/c) is not used because it is constant in all mixes.

It should be noted here that all inputs (variables) (v1, v2, v3) have been converted from actual values to relative values ranging from (0, 1) as required by the SPSS program during the training period So that the value of output is relative, to obtain actual values of outputs (diameter of flow) must be modification by using the Eq. (6), to return them to their actual value.

$$Scaled\ Value = \frac{X - Xmin}{Xmax - Xmin} \tag{6}$$

Thus, the output values (diameter of flow) can be deduced using the Eq. (7) and Eq. (8):

$$y = \frac{47.5}{1 + e^{-(2.201 + 4.167 * \tanh(X))}} + 252.5 \tag{7}$$

where,

$$X = 69.976 - \left(2.18 * \frac{W}{C}\right) + \left(0.184 * \frac{F}{c}\right) - \left(30.333 * \frac{S}{c}\right) \tag{8}$$

In the practical application of Eq. (6) and Eq. (7) using one of the experimental data when (w/c) is equal to (0.55), (f/c) is equal to (0.2%), and the (s/c) is equal to (1.697%). As a result, the diameter of flow measured from Eq. (6) and Eq. (7) is equal (218.6 mm).

The validation model for the extracted values were based on statistical criteria (mean absolute percentage error (MAPE), average accuracy percentage (AA%), the coefficient of determination (R^2), and the coefficient of correlation (R) to prove the efficiency of the Equation derived from the ANNs model, where the value of (MAPE) was calculated by Eq. (9).

$$MAPE = \frac{\left(\frac{\sum |A - E|}{A}\right) * 100}{n} \tag{9}$$

where,

A: Actual values of flow diameter.

E: The values of flow diameter are calculated by Eq. (8).

n: Number of samples.

The average accuracy percentage (AA%) value is calculated by Eq. (10).

$$AA\% = 100\% - MAPE \tag{10}$$

Table 5 shows the results of statistical standards for the validation model to number (1) sample, which represents the ratio (4%) from total samples; the results show that the Equation used to estimate the flow diameter in the ANNs model has a high accuracy of (97.53%), that accuracy is considered excellent for the efficiency of the model which developed in the research.

6.2.2 Flow time

The input data, as mentioned above, are (w/c), (f/c), and

(s/c), while the value extracted from the output layer is the flow time. Table 6 shows the ratios of the data division in the training group, testing group, and validation group. The results showed that the best data division when the training group (88%), the testing group (8%), and the validation group were equal (4%) because they have the highest ratio of coefficient correlation (95.7%) and the lowest error ratio (1.7%). So, the striped method was used because it gives the highest coefficient of correlation and the lowest error ratio.

Based on Eq. (2) and the observation of Table 7, the neuron nodes were divided into the hidden layer (middle). Thus, the batter number of neuron nodes was a single neuron node because it gives the highest coefficient of correlation (95.7%) and the lowest error ratio (1.7%), that values get it when the learning rate is 0.4, and the momentum term equal to 0.9, so the type of transfer function for middle layer was sigmoid.

Table 5. The result validation of ANNs model

Statistical Standards	Correlation Coefficient (R)	Determination Coefficient (R2)	Mean Absolute Percentage Error (MAPE)	Average Accuracy Percentage (AA%)
Statistical value for ANNs model	96.6	89.4	2.47	97.53

Table 6. The effect of data division on the performance of the ANNs for flow time

Data Division			Training Error%	Testing Error%	Coefficient Correlation (r)%
Training%	Testing%	Validation%			
80	8	12	7.7	14.6	96.7
80	16	4	7.3	3.2	97.1
76	12	12	6.3	22.3	96
68	16	16	8.1	4.9	96.7
68	20	12	7.2	10.8	96.2
76	20	4	9	22.1	94.4
88	8	4	9.2	1.7	95.7
84	8	8	8.1	5.8	96.2
60	20	20	9.9	23.8	93.1
76	12	12	9.4	15.7	95.4

Table 7. The number of nodes in the hidden layer on the performance of the ANNs

No. of Nodes	%Training Error	%Testing Error	Coefficient Correlation (r)%
1	9.2	1.7	95.7
2	2.6	8.1	98.2
3	7.9	1.9	96.1
4	8.1	3.2	96.6
5	4.9	2.2	97.4
6	2.5	2.8	98.7
7	4.4	7.0	98.1

The weights of the bond between the neurons of layers and the threshold limits of the hidden layer and the output layer are shown in Figure 6.

The final Eq. (11) and Eq. (12) to estimate the flow time of the SCM through the mini V-funnel were deduced through the correlation weights, and the threshold limits and modification of the relative values to actual values were calculated by using Eq. (6), that previously mentioned.

$$y = \frac{4.7}{1 + e^{(2.399+3.813*\tanh(X))}} + 13.4 \quad (11)$$

where,

$$X = 83.242 - \left(2.173 * \frac{W}{C}\right) + \left(0.332 * \frac{F}{c}\right) - \left(0.102 * \frac{S}{c}\right) \quad (12)$$

The practical application of Eq. (11) and Eq. (12) was based on one of the practical experiments, when the values of (w/c), (f/c), and (s/c) equal to (0.57), (0.2%) and (1.697) respectively, the results of estimated flow time, that calculated from the Eq. (11) and Eq. (12) equal to 15.76 seconds. At the same time, the actual flow time was equal to 15.20 seconds.

Table 8 shows the results of the statistical standards of the validation model for many (1) samples that represent the percentage (4%) from the total samples data selected from the division model; the results show that the Equation used to estimate the flow diameter in ANNs model has a high accuracy of (91.85%), that accuracy is considered excellent for the efficiency of the model developed in the research.

Table 8. The result validation of ANNs model

Statistical Standards	(R)	(R2)	(MAPE)	(AA%)
Statistical value for ANNs model	95.70	87.30	8.150	91.850

7. CONCLUSIONS

(1) Add the carbon fiber to the self-compact mortar with a rise (f/c) ratio, the flowing diameter reduces, and the travel times through the funnel increase. Increasing the ratio of water to cement (w/c) increased the flow diameter while it was within the acceptable bounds whenever the (w/c) was equal to 0.57 and 0.6, as well as the (w/c) was equal to 0.65, and the mixture was bleeding.

(2) Increasing the (w/c) resulted in a higher flow time within the specified range once the (w/c) were set to 0.57, 0.6, and 0.65.

(3) The neural network approach (ANN) was employed to estimate the flow diameter with such a significant level of overall accuracy rate (97.53%) and correlation coefficient (96.6%), in addition to the flow duration with a high degree of overall accuracy rate (91.85%) and correlation evaluation (95.7%).

(4) The artificial neural network model showed that it is relatively insensitive to the number of hidden layer neural nodes.

REFERENCES

[1] Lozano-Lunar, A., da Silva, P.R., De Brito, J., Fernández, J.M., Jiménez, J.R. (2019). Safe use of electric arc furnace dust as secondary raw material in self-compacting mortars production. Journal of Cleaner Production, 211: 1375-1388. https://doi.org/10.1016/j.jclepro.2018.12.002

[2] Karataş, M., Benli, A., Ergin, A. (2017). Influence of ground pumice powder on the mechanical properties and durability of self-compacting mortars. Construction and Building Materials, 150: 467-479. https://doi.org/10.1016/j.conbuildmat.2017.05.220

[3] Benabed, B., Kadri, E.H., Azzouz, L., Kenai, S. (2012). Properties of self-compacting mortar made with various types of sand. Cement and Concrete Composites, 34(10): 1167-1173. https://doi.org/10.1016/j.cemconcomp.2012.07.007

[4] Silva, P.R.D., Brito, J.D. (2015). Fresh-state properties of self-compacting mortar and concrete with combined use of limestone filler and fly ash. Materials Research, 18: 1097-1108. https://doi.org/10.1590/1516-1439.028715

[5] Bissonnette, B., Pierre, P., Pigeon, M. (1999). Influence of key parameters on drying shrinkage of cementitious materials. Cement and Concrete Research, 29(10): 1655-1662. https://doi.org/10.1016/S0008-8846(99)00156-8

[6] Rozière, E., Granger, S., Turcry, P., Loukili, A. (2007). Influence of paste volume on shrinkage cracking and fracture properties of self-compacting concrete. Cement and Concrete Composites, 29(8): 626-636. https://doi.org/10.1016/j.cemconcomp.2007.03.010

[7] Johansen, R., Dahl, P.A., Skjolvold, O. (1993). Control of plastic shrinkage in concrete at early ages. 18th Conference on Our World in Concrete & Structures, 25(27): 149-154.

[8] Safiuddin, M., Abdel-Sayed, G., Hearn, N. (2010). High performance mortar with carbon fibers: Properties and mix optimization. LAP Lambert Academic Publishing.

[9] Chung, D.D.L. (2000). Cement reinforced with short carbon fibers: a multifunctional material. Composites Part B: Engineering, 31(6-7): 511-526. https://doi.org/10.1016/S1359-8368(99)00071-2

[10] Wang, C., Li, K.Z., Li, H.J., Jiao, G.S., Lu, J., Hou, D.S. (2008). Effect of carbon fiber dispersion on the mechanical properties of carbon fiber-reinforced cement-based composites. Materials Science and Engineering: A, 487(1-2): 52-57. https://doi.org/10.1016/j.msea.2007.09.073

[11] Gao, J., Wang, Z., Zhang, T., Zhou, L. (2017). Dispersion of carbon fibers in cement-based composites with different mixing methods. Construction and Building Materials, 134: 220-227. https://doi.org/10.1016/j.conbuildmat.2016.12.047

[12] Graupe, D. (2013). Principles of Artificial Neural Networks (Vol. 7). World Scientific.

[13] Begg, R., Kamruzzaman, J., Sarker, R. (2006). Neural Networks in Healthcare: Potential and Challenges: Potential and Challenges. IGI Global.

[14] Zhang, L. M., Cong, Y., Meng, F. Z., Wang, Z. Q., Zhang, P., Gao, S. (2021). Energy evolution analysis and failure criteria for rock under different stress paths. Acta Geotechnica, 16(2), 569-580. https://doi.org/10.1007/s11440-020-01028-1

[15] Sagban Saadoon, A., Sami Malik, H. (2017). Prediction of ultimate load of concrete beams reinforced with FRP bars using artificial neural networks. Al-Qadisiyah Journal for Engineering Sciences, 10(1): 11-25. https://qjes.qu.edu.iq/article_123382.html.

[16] Zhang, L.M., Wang, X.S., Cong, Y., Wang, Z.Q., Liu, J. (2023). Transfer mechanism and criteria for static–dynamic failure of granite under true triaxial unloading test. Geomechanics and Geophysics for Geo-Energy and Geo-Resources, 9: 104. https://doi.org/10.1007/s40948-023-00645-w

[17] Efnarc, S. (2002). Guidelines for Self-Compacting Concrete. London, UK: Association House.

[18] Mehdipour, I., Libre, N.A., Shekarchi, M. (2011). Development of Fiber reinforced SCM for sustainable construction. Journal of Structural Engineering and Geotechnics, 1(1), 19-29.

[19] Iraqi Standard no. 5 for the year 1984, "Portland Cement," "Natural Aggregate used for Concrete and Construction," and Central Organization for Standardization and Quality Control, Baghdad. https://www.hrw.org/reports/pdfs/i/iraq/iraq938.pdf.

[20] ASTM C 494, "Standard Specification for Chemical Admixtures for Concrete," Annual Book of ASTM Standards, Vol. 04.02, 2004; pp. 1-5. https://www.astm.org/c0494_c0494m-19e01.html.

[21] Zhang, L.M., Chao, W.W., Liu, Z.Y., Cong, Y., Wang, Z.Q. (2022). Crack propagation characteristics during progressive failure of circular tunnels and the early warning thereof based on multi-sensor data fusion. Geomechanics and Geophysics for Geo-Energy and Geo-Resources, 8: 172. https://doi.org/10.1007/s40948-022-00482-3

[22] Zurada, J. (1996). Introduction to Artificial Neural System. Jaiur Publishing House. https://dl.acm.org/doi/abs/10.5555/131393